Radio Frequency Interference Validation Testing for LAAS using the Stanford Integrity Monitor Testbed

Ming Luo, Gang Xie, Dennis Akos, Sam Pullen, Per Enge
Stanford University

ABSTRACT

Since GPS signals have very low received power levels (–130 dBm, or –160 dBW), their vulnerability to RF Interference (RFI) is a serious concern. This is particularly true for GPS-based safety-critical systems such as the Local Area Argumentation System (LAAS). The Stanford LAAS Integrity Monitor Testbed (IMT) is a prototype of a LAAS Ground Facility (LGF) that is composed of various monitors to detect possible hazardous anomalies for LAAS users. The goals of this study are to validate the IMT detection algorithms under various RFI conditions, to evaluate the RFI mask specified by the LAAS MOPS, to explore new algorithms for improved RFI detection, and to improve the system robustness under RFI.

RFI can be categorized into three main types: broadband, continuous wave (CW), and pulsed interference. Multiple GPS performance metrics may be affected by RFI, including pseudorange and carrier-phase measurement accuracy, phase lock status, acquisition time, etc. The current IMT has several integrity monitors that are designed to detect anomalies that may affect pseudorange and/or carrier phase measurements and their error statistics. Any serious degradation caused by RFI should be detectable before a hazardous error occurs. In addition, Automatic Gain Controller (AGC) outputs from the IMT receivers are sensitive to interference but are not sensitive to other types of failures. In addition to being more sensitive to changes in RFI, they provide a useful metric for Executive Monitoring (EXM) to distinguish between RFI, satellite failures, and IMT receiver failures.

A single GPS receiver, one of the three used in the IMT, has been tested under the RFI test conditions specified by FAA AOS-240. These tests are used to validate performance against the LGF Specification RFI requirements. Careful receiver calibration was conducted prior to testing, and each test condition (such as GPS power) was adjusted accordingly. Subsequently, the full IMT is tested with selected RFI scenarios to measure the response of the multiple antenna, multiple receiver LGF implementation. This also tests the ability of EXM to exclude the affected measurements. The AGC outputs are also evaluated and compared with the IMT monitors.

We have found that the current receivers tested comply with the MOPS mask with respect to in-band and near-band CW interference. However, the tolerance of out-of-band CW is slightly less than the mask level. Also, it appears that the existing IMT monitors are no better RFI detectors than the receiver loss-of-lock indicator. AGC is sensitive to both wide band noise and CW interference. In addition, AGC is also useful separate RFI from other failure modes that can be detected by the IMT.

1.0 INTRODUCTION

As a result of the low (–130 dBm, or –160 dBW) received power levels of GPS [1], their vulnerability to RF Interference (RFI) is a serious concern, particularly for GPS-based safety-critical systems such as the Local Area Argumentation System (LAAS). The interference can result in degraded navigation accuracy or complete loss of receiver tracking. There are various types of interference sources that may be intentional or unintentional. These include: out-of-band emissions from adjacent bands, harmonics and intermodulation products, pulsed interference from radar signals, accidental transmission by experiments, and hostile jamming. Depending on its bandwidth, RFI interference can be classified as broadband, narrowband, or as a CW tone at a single frequency. The interference can be pulsed with a certain duty cycle or be continuous. Among those types, a CW tone that coincides with that of a GPS signal (called "coherent") is most devastating [2] because of the line structure in GPS signals.

Since the effect on a GPS receiver strongly depends on the types of the interference, RTCA developed interference masks in its Minimum Operational Performance Standards (MOPS) for LAAS and WAAS to reflect the design requirement respectively [3-5]. Figure 1 is the RF interference mask published in the MOPS. The mask gives an overall picture of the interference levels at which a compliant receiver will still provide nominal performance. For example, the maximum broadband interference source power level for nominal performance is specified to be –110.5 dBm/ MHz. For CW tones near the L1 carrier frequency, the upper limit is –120.5 dBm.

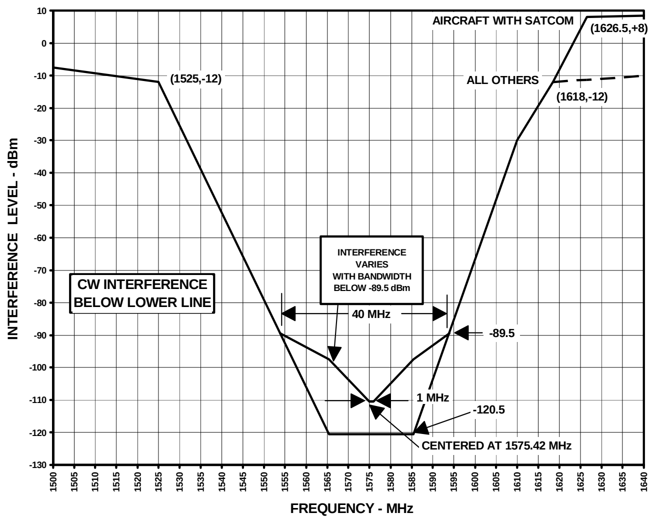

Figure 1: RTCA MOPS RFI Mask

Much effort has been invested to protect GPS against RF interference. The GPS frequency band has been protected by international and Federal Communications Commission (FCC) frequency assignments. In addition, GPS uses a spread-spectrum modulation that has RFI advantages over narrow-band systems. Various techniques have been developed to make GPS receivers work more robustly in the presence of RFI including: adaptive antennas and antenna arrays, RF/IF filtering, code/carrier tracking aiding and enhancement, integration GPS with inertial sensors, etc. One of the major goals of GPS modernization (which will include such aspects as additional signals, wider spread spectrum/higher code rates, and higher power level) is to improve RFI-resistance properties.

In addition to the above mitigation techniques, it is important to detect the presence of RFI that cannot be mitigated in order to protect the safety-of-life service. The goals of this research are to evaluate candidate RFI detectors, to examine the susceptibility mask of the IMT reference receivers, and to eventually improve LAAS system robustness to RFI.

2.0 CANDIDATE RFI DETECTORS

2.1 Common Receiver Observables

Most GPS receivers report Carrier-to-Noise (C/N_o) ratio as one of their observables. Although the specific method of C/N_o estimation may differ from one manufacturer to another, they are similar in the first order. In the presence of RFI, the equivalent carrier signal to noise ratio can be expressed as [2]:

$$[c/n_0]_{eq} = \frac{1}{\dfrac{1}{c/n_0} + \dfrac{j/s}{QR_c}} \qquad (1)$$

where:

c/n_0 carrier-to-noise ratio without interference;

j/s jammer-to-signal power expressed as a ratio;

R_C GPS PRN code chipping rate (1.023×10^6 chips/sec for C/A code);

Q spread spectrum-processing gain (1 for narrowband and 2 for wideband Gaussian).

In terms of dB-Hz, the equation becomes:

$$[C/N_0]_{eq} = -10\log\left[10^{-(C/N_0)/10} + \frac{10^{(J/S)/10}}{QR_c}\right] \qquad (2)$$

where:

C/N_0 carrier-to-noise ratio without interference, in dB-Hz (= $10\log(c/n_o)$)

J/S jammer-to-signal power ratio, in dB (= $10\log(j/s)$)

A plot of equivalent signal-to-noise ratio vs. jammer power (based on equation 2) is shown in Figure 2. The noise power n_0 is set to be at –110 dBm/ MHz. GPS power was set to be –130 dBm, –125 dBm, and –120 dBm, respectively. Obviously when jammer power increases relative to the signal power, the equivalent signal-to-noise ratio decreases. When the equivalent carrier-to-noise ratio is lower than the tracking threshold (e.g., specified to be 32 dB-Hz for a NovAtel narrow-correlator receiver), receivers lose lock and can no longer continually track the satellite.

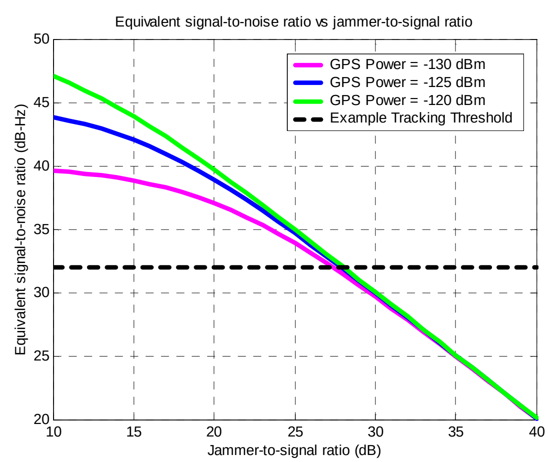

Figure 2: C/N_0 vs. Jammer-to-Signal Ratio

In addition to C/N_0, some receivers also report accumulated lock time, which resets whenever the receiver detects a possible cycle slip. The reset of lock time may indicate the presence of RFI. When the RFI power increases further, the receiver will lose the ability to track the satellite. Therefore, receiver loss-of-lock can also be an indicator of RFI.

2.2 Existing IMT Monitors

The Stanford LAAS Integrity Monitor Testbed (IMT) is a prototype of the LAAS Ground Facility (LGF) that is composed of various monitors. Each monitor is designed to target at a different failure mode that may threaten LAAS users, such as GPS signal deformation, ephemeris anomalies, code-carrier divergence, receiver problems, etc. Depending on the type and strength of the RFI, it may impact one or more existing IMT monitors. Once a monitor is affected, it may issue an alert despite not being designed specifically to address RFI. Several monitors that have the potential to detect RFI are described below. More complete information on the IMT and its monitors and test metrics can be found in [6].

SNR (*Signal-to-Noise Ratio*): This function is designed to detect GPS satellite signal power anomalies. It takes a moving average of receiver-reported C/N_0. SNR is a smoothed version of C/N_0; therefore its relationship with RFI should follow a trend similar to that shown in Figure 2. The threshold for this test was established based on nominal IMT data and varies with satellite elevation, as the C/N_0 statistic is noisier at lower elevation angles.

MQM (*Measurement Quality Monitoring)*: This function is designed to detect sudden jumps or rapid accelerations in carrier phase measurements. Before carrier smoothing occurs on each epoch, the last 10 epochs (5 seconds) of carrier phase measurements of all ranging sources being tracked are used to fit the following 2nd-order model:

$$\phi^* = \phi_0^* + \frac{d\phi^*}{dt}\Delta t + \frac{d^2\phi^*}{dt^2}\frac{\Delta t^2}{2}; \qquad (3)$$

where:

$$\phi^* = \phi - \phi^{corr} - \phi^{ave} = \hat{\phi} - \phi^{ave} \; ; \qquad (4)$$

$$\phi^{ave} = \frac{1}{N_c}\sum_{i=1}^{N_c}\phi_i \; ; \qquad (5)$$

$$\phi^{corr} = R^{SV} + \tau^{SV} ; \qquad (6)$$

N_c is the number of satellites tracked by the receiver, and R^{SV} and τ^{SV} are the user-to-satellite range and satellite clock corrections, respectively. Three test statistics are defined:

$$Step\,test \;\equiv\; \phi^*_{meas} - \phi^*_{pred} ; \qquad (7)$$

$$Ramp\;\; test \;\equiv\; \frac{d\phi^*}{dt} \qquad (8)$$

$$Acceleration\; test \;\equiv\; \frac{d^2\phi^*}{dt^2} ; \qquad (9)$$

where ϕ^*_{meas} is the computed value of ϕ^* at the current epoch, and ϕ^*_{pred} is the value computed from (3) based on the coefficients ϕ_0^*, $\frac{d\phi^*}{dt}$, and $\frac{d^2\phi^*}{dt^2}$ computed from a least-squares fit to the last 10 phase measurements.

Because the presence of RFI will increase the noise in phase tracking, and RFI that is immediately hazardous is likely to suddenly and significantly affect the carrier-phase measurements, it is expected that all three MQM test statistics (Step, Ramp, and Acceleration) would respond to varying degrees.

Innovation Test: In the IMT, pseudorange measurement is smoothed by carrier phase measurement using the following filter:

$$PR_s(k) = \frac{1}{N_s}PR(k) + \frac{N_s - 1}{N_s}[PR_s(k-1) + \phi(k) - \phi(k-1)] \quad (10)$$

where:

$PR_s(k)$	Carrier Smoothed Code (CSC) at k^{th} epoch.
$PR(k)$	raw pseudorange measurement at k^{th} epoch.
N_s	smoothing filter time constant (200 epochs, or 100 seconds)
$\phi(k)$	carrier phase at k^{th} epoch.

Both the airborne user and the LGF apply first-order carrier smoothing using (10) with the same smoothing time constant. After smoothing is completed on a given epoch, the MQM innovation test statistic is computed to detect unusual pseudorange deviations:

$$Inno(k) \equiv PR(k) - \left(PR_S(k-1) + \phi(k) - \phi(k-1)\right) \quad (11)$$

As can be seen from Equation (11), the innovation test statistics is strongly dependent on pseudorange noise. The relationship between pseudorange variance and broadband RFI can be expressed as the following equation [7]:

$$\sigma_k^2 = \frac{d(cT_c)^2 BW_L}{2\left[\frac{C(el^k)}{N_o + I_o}\right]}\left[1 + \frac{2}{\left[(2-d)\frac{C(el^k)}{(N_o + I_o)}\right]T_{square}}\right] \quad (12)$$

where:

d	correlator spacing
c	speed of light, approx. 3×10^8 m/s
T_c	C/A code chip width = 1 µs
BW_L	1 sided tracking loop bandwidth
T_{square}	squaring loss, from early-late power detector
$C(el^k)$	carrier power of the k^{th} satellite, in dBm
N_0	noise power, in dBm/Hz
I_0	interference power, in dBm/Hz

Clearly the presence of interference decreases the equivalent signal-to-noise ratio and therefore increases the pseudorange covariance. A NovAtel OEM4 receiver implementation can be used as an example: $d = 0.1$ chip, $BW = ½$ (2 seconds of carrier smoothing), $T_{square} = ½$. The noise is assumed at the level of –110 dBm/ MHz.

For the case of broadband interference (bandwidth > 20 MHz around L1), the pseudorange accuracy vs. interference is plotted in Figure 3. When the interference is low relative to the noise power, accuracy degrades slowly when interference increases. When the interference is comparable or higher than the noise level, accuracy is impacted dramatically. Accuracy is also a function of GPS power. Three GPS power levels are shown in the plot: –130 dBm, –125 dBm, and –120 dBm. Obviously, when the GPS power is high, it takes more interference to degrade the pseudorange accuracy.

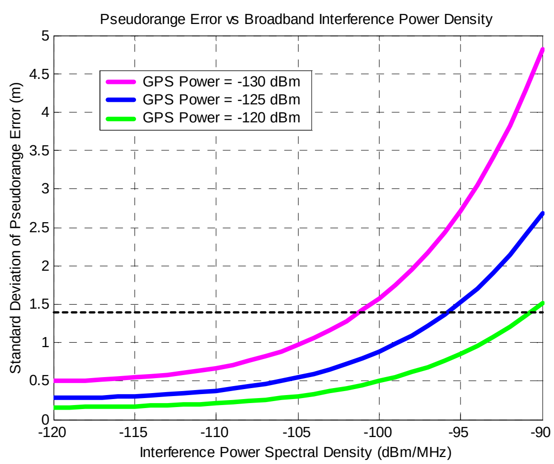

Figure 4: Standard Deviation of Pseudorange Error vs. Broadband RFI Power

It is expected that the stronger the RFI, the greater the variance of pseudorange measurements and the noisier the IMT innovation test. Therefore, the threshold may be exceeded more frequently and the flags will be more likely to be seen. In addition, if RFI is severe enough to suddenly change raw pseudorange measurements significantly, it will be observable by this test.

2.3 Automatic Gain Control (AGC)

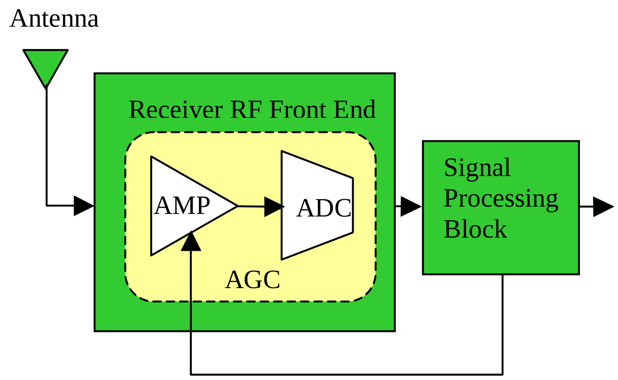

Figure 3: AGC Block Illustration

Although not commonly accessible by users, Automatic Gain Control (AGC) is widely implemented in modern GPS receivers. AGC is used to adjust the input signal gain so that the Analog-to-Digital Converter (ADC) can be optimally configured. The AGC is based on the distribution of the ADC output and is PRN independent. A simplified block diagram illustrates the function of AGC in Figure 4. Since the GPS signal is below the noise floor, the AGC gain reflects the noise level at the input and therefore can be used to detect the presence of RFI.

3.0 SINGLE CHANNEL RFI TESTING

In order to conduct RFI testing in a controlled environment, a single-channel GPS simulator is used with a single NovAtel OEM4 GPS receiver. The test setup is shown in Figure 5. The HP 8648B is used to generate controlled CW interference. A WelNavigator broadband noise source is used to generate Wide Band (WB) noise, and the bandwidth is limited to 24 MHz via an L1 bandpass filter. A programmable attenuator is employed to control the power level of the interference. The CW or WB signal is combined with the GPS signal from the simulator and is then input into the receiver. The GPS signal power (PRN 1 is used) is kept at –130 dBm during all of the tests. All C/N_0, range measurements, and AGC packets are recorded for post-processing.

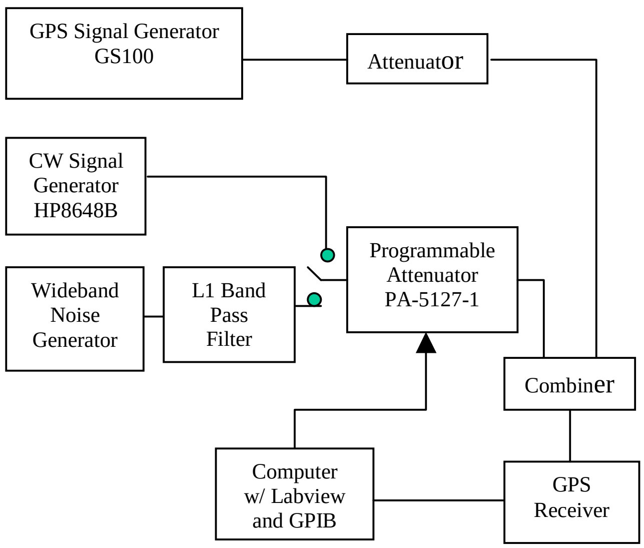

Figure 5: Test Setup for Single Receiver with Single-Channel Simulator

The RFI test cases were chosen around the corners of the mask shown in Figure 1. Each of the cases of interest is listed in Table 1, and this paper includes results for the highlighted cases. During the test for each case, the RFI power is not fixed to the level specified in the table. Instead, it starts at a lower level and gradually increases until the receiver loses lock.

Test Case	RFI Frequency (MHz)	Bandwidth (kHz)	RFI Power (dBM)
1	1575.42	CWI	-114.5
2	1555.42	CWI	-83.5
3	1595.42	CWI	-83.5
4	1610	CWI	-24.0
5	1525	CWI	-6.0
6	1618	CWI	-6.0
7	1575.42	3	-112
8	1575.42	100	-104.5
9	1575.42	20,000	-91.5
10	1575.42	Pulse length 1 ms, 10% duty cycle	+20.0
11	1575.42	Pulse length 1 ms, 10% duty cycle	+30.0

Table 1: RFI Test Cases

The wideband noise RFI (Case #9) was tested first, and the results are shown in Figure 6. The first subplot shows the RFI Power Spectral Density (PSD) injected into the system. As can be seen, the PSD starts at –114.5 dBm/MHz and increases by 1 dB each hour. The black dash line indicates the Mask level of –110.5 dBm/MHz. The green curve in the second subplot is the lock time observable. It resets at the RFI power of –106.5 dBm/MHz which indicates a possible cycle slip at that point.

The blue trace in the third subplot is C/N_0 with units of dBHz. When the RFI power is low, C/N_0 remains at about 36 dBHz. When RFI power increases, C/N_0 gradually decreases. If a threshold is set to be approximately 6 times the standard deviation, it is estimated that the C/N_0 would likely exceed the threshold at an RFI power of –108.5 dBm/MHz. It is recorded (not shown in this plot) that the receiver completely lost lock at an RFI power of –103.5 dBm/MHz.

The last subplot shows the AGC response. If the same criteria (6 times the standard deviation) is used to set the threshold, it is estimated that AGC would trigger the flag at an RFI power of –111.5 dBm/MHz (or –97.7 dB total in the 24-MHz-wide L1 band). Note that this level is improved over the one specified by the mask. It indicates that in this case, AGC could detect a problem before the MOPS upper limit is reached. However, since it is desired that the system continue to operate normally up to this limit, the actual AGC threshold would be set to alert at a broadband RFI level slightly higher than the limit.

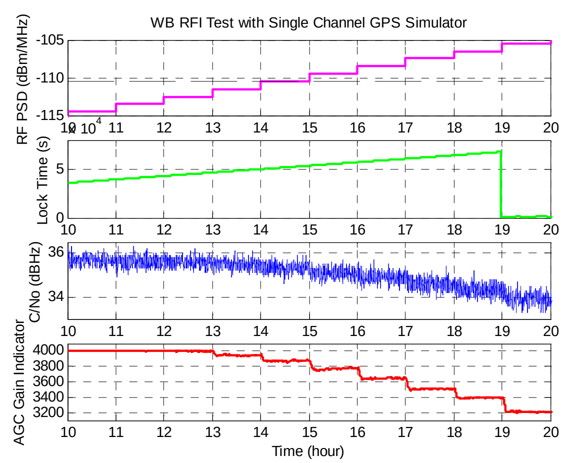

Figure 6: Test Results of WB Noise (Case #9)

The order of detection from this test is summarized in Table 2. As noted above, the AGC responds first, C/N_0 is second, followed by the cycle slip indicator, and receiver loss of lock is the slowest.

Observable	AGC	C/N_0	Lock Time (Cycle Slip)	Loss of Lock
RFI PSD (dBm/MHz)	-111.5	-108.5	-106.5	-105.5

Table 2: Order of Detection of WB RFI, Case #9

The next case tested is in-band CW interference. The frequency is set to be 1075.42302 MHz, i.e., 3020 kHz offset from L1 [3]. The offset is chosen such that the CW is not co-located with the strongest GPS spectral line. As a result, the impact of the interference injected in this test is more benign than the worst case. In the real world, the GPS spectral lines shift due to the Doppler effect. A CW jammer with a fixed frequency might then cross the worst spectral lines of one or more satellites, leading to a much more severe impact. Note that it is possible to simulate the scenario by sweeping the CW frequency while synchronizing the receiver clock with the simulator clock. The results then would reflect reality more closely.

The CW test results are plotted in Figure 7. Similar to Figure 6, the four subplots show injected CW interference power, lock time, C/N_0, and AGC, respectively. The order of RFI detection is: AGC, C/N_0, cycle slip, and loss of lock – the same as the WB noise case. In this case, AGC can detect RFI at the power of –101 dBm, which is 9 dB higher than the level specified in the mask (–120 dBm). Note that in the WB noise case described previously, AGC can detect RFI at the power level of –111.5 dBm/MHz, or, –97.7dBm total in the L1 band. By comparing the total in-band interference energy, it appears that AGC is about 3 dB more sensitive in detecting CW than WB.

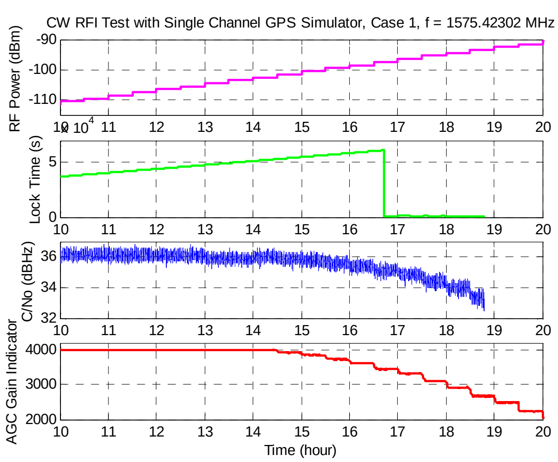

Figure 7: RFI Test with CW Interference, Case #1

Figure 8 showed the results of CW interference for Case #3. The frequency of the CW is now at 1595.42 MHz, i.e., 20 MHz above the GPS L1 frequency, and is likely attenuated by the front end of the GPS receiver. Note that in this case, C/N_0 can detect RFI at the power level of about –48 dBm while AGC would flag at –44 dBm. Thus C/N_0 detects the RFI earlier than AGC. The order of responses is: C/N_0, AGC, cycle slip, then loss of lock.

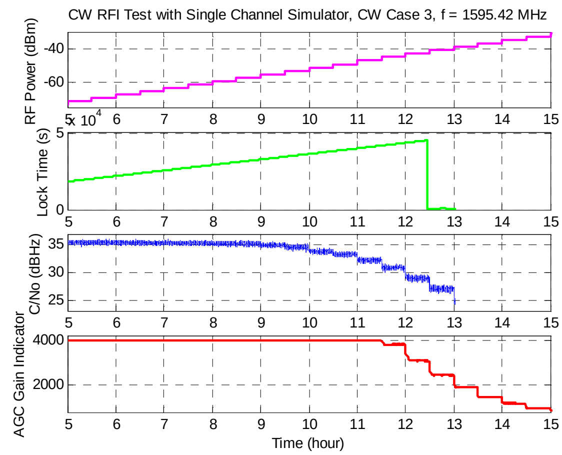

Figure 8: RFI Test with CW Interference, Case #3

Instead of showing results for all of the cases tested, the receiver susceptibility mask is summarized in Figure 9. The black line re-plots the mask level for CW interference. The green curve shows the power level at where the receiver loses lock. The AGC and C/No detection levels are drawn in red and blue, respectively. Based on these results, cycle slip is not as sensitive as AGC or C/No in all cases. For clarity, it is not included in this summary plot.

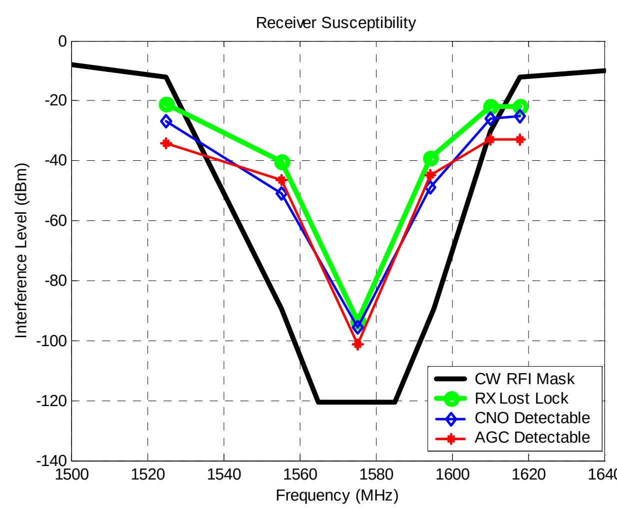

Figure 9: Receiver Susceptibility Summary

As can be seen, with in-band and near-band CW interference, the power level that the receiver can tolerate is much higher (10-20 dB) than the mask level. With CW at frequencies far away from L1 (defined by outside the expected receiver bandwidth), the receiver loses lock at interference levels below those of the mask. In order to be fair, the RFI impact may not be as severe in real applications since the GPS antenna can further filter out out-of-band RFI. Neglecting the performance of the receiver with respect to the mask, it can be noted that in all cases tested, the receiver can detect the RFI before it loses lock. The order of detection between AGC and C/N_0 varies with CW frequency.

4.0 RFI TESTING WITH LIVE GPS SIGNALS AND THE IMT

In order to conduct RFI testing in a more realistic environment and to validate the IMT performance under RFI, tests were also conducted with the full three-receiver IMT setup. The test configuration is illustrated in Figure 10. GPS signals come from three separated NovAtel Pinwheel antennas that are installed on the rooftop of the LAAS lab. The signal from antenna #1 is combined with RFI before it is passed into receiver #1. Signals from antennas #2 and #3 are directly connected to receiver #2 and #3. A low-noise amplifier is used after each antenna to overcome cable losses. As with the single-receiver tests, WB noise is generated using the WelNavigate broadband noise source, and CW interference is generated using the HP 8648B. Either WB or CW is injected into the system during the test (not both at the same time). The IMT takes observables from its three reference receivers and passes them to a series of the integrity monitors tied together by executive monitoring (EXM), which translates flags into decisions to exclude specific faulted measurements. The IMT outputs flags, test statistics, and corrections for approved satellites at a rate of 2 Hz.

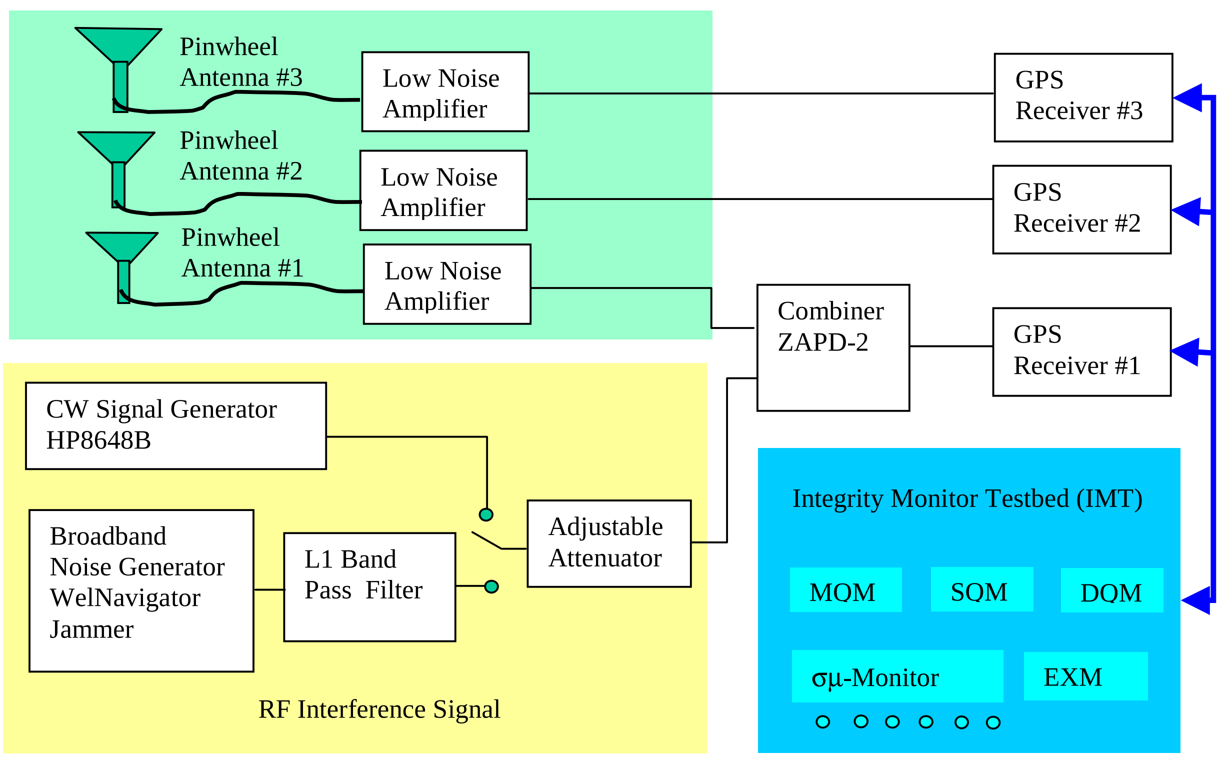

Figure 10: RFI Test Setup with Live GPS Signals and IMT

4.1 WB Test Results

WB RFI is injected in the tests described in this section. IMT outputs and AGC packets are examined separately. In all the following results, the plots are of a consistent nature. The first subplot presents the injected RFI PSD vs. time, and the lower subplot(s) show test statistic responses vs. time. Figure 11 shows the IMT SNR results of satellite PRN 6. The threshold is also plotted as a black dashed line. As can be seen, the SNR responds to RFI and exceeds the threshold when RFI power increases to –95 dBm/ MHz. Note that there is no SNR data for a period of time when RFI power is at –85 dBm/MHz. That is because the receiver loses track of this satellite due to the injected RFI.

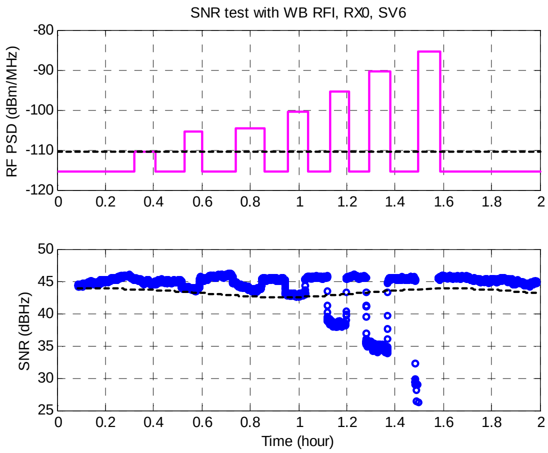

Figure 11: IMT SNR Results with WB RFI

The IMT MQM results are presented in Figure 12. The acceleration (Acc) and innovation (Inno) test statistics are shown in the second and the third subplot, respectively. The thresholds are also plotted in black dashed lines for comparison. As noted in Section 2, both test statistics become noisier with the presence of RFI. In the case of Inno, the variation of the test statistics increases such that the threshold is crossed at an RFI power level of –90 dBm/MHz. However, in the case of Acc, though the variation increases noticeably, the test statistic never exceeds the threshold. When the RFI power is increased to –85 dBm/MHz, the receiver loses lock.

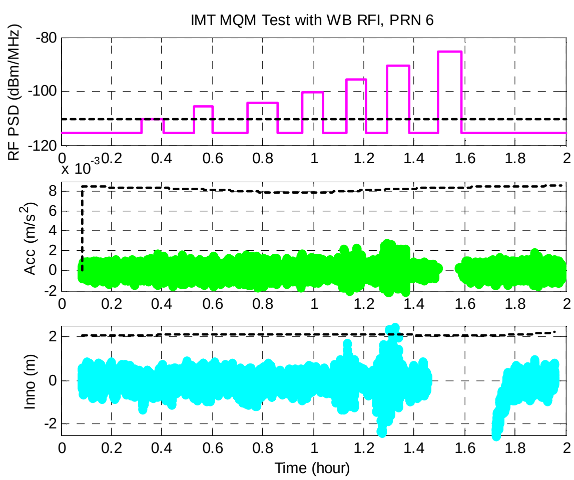

Figure 12: IMT Acc and Inno Tests with WB RFI

The AGC test result with WB RFI is shown in Figure 13. The threshold is established at six times the standard deviation of nominal data. The AGC monitor can flag when the RFI is as low as –110 dBm/MHz, which is very similar to the result obtained in single-receiver testing. This confirms that, in this more realistic setup, AGC remains a very sensitive RFI detector.

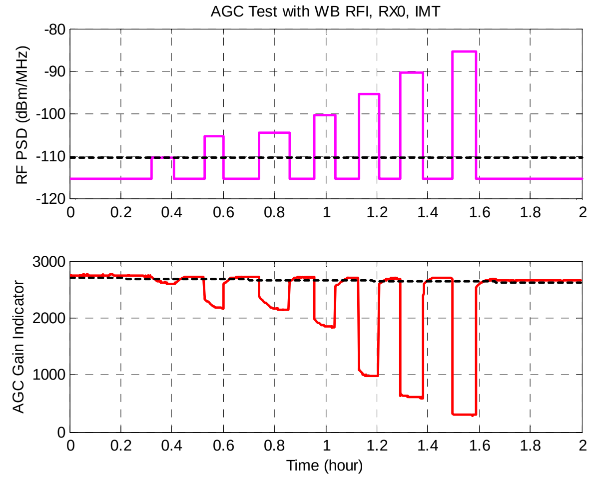

Figure 13: IMT AGC Results with WB RFI

4.2 CW Test Results

Test results with CW RFI are presented in this section. Figure 14 shows the IMT SNR test statistics on PRN 6 (at an elevation angle of about 60°) and PRN 29 (at an elevation angle of about 30°). As can be seen, satellite PRN detects RFI at –110 dBm, while PRN 29 (~30 degree) loses lock without detection. That is because the SNR test statistic for a low-elevation satellite is noisier. Therefore its threshold is set further from the mean of the nominal data. It thus has less chance to flag the presence of RFI than a satellite at a higher elevation. However, since lower-elevation satellites have larger nominal range errors and are thus deweighted in user navigation solutions, failures on lower-elevation satellites must be more severe (and thus more detectable) to create a threat to LAAS users.

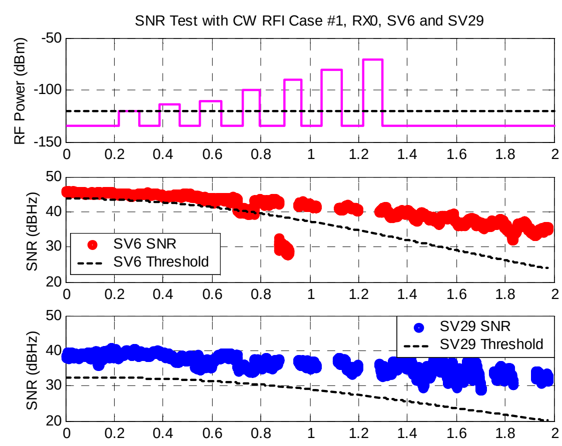

Figure 14: IMT SNR Test Results with CW RFI

The IMT MQM test results are shown in Figure 15. The acceleration (Acc), Ramp, and Step test statistics are displayed in subplots 2, 3 and 4, respectively. Unlike the WB RFI case, the standard deviations of these test statistics do not get larger due to RFI. This is likely due to the fact that, as noted above, no C/A code spectral line is crossed by this interference; thus little impact on IMT carrier-phase measurements is expected. However, when the RFI power increases to –95 dBm or greater, the receiver loses lock. In this case, MQM is not a better RFI detector than the receiver's own loss-of-lock indicator.

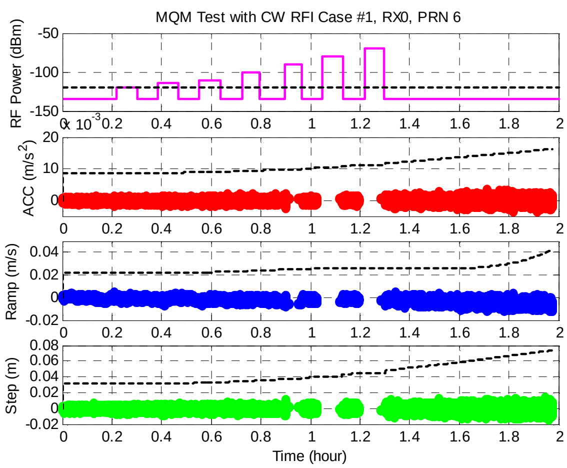

Figure 15: IMT MQM Results with CW RF

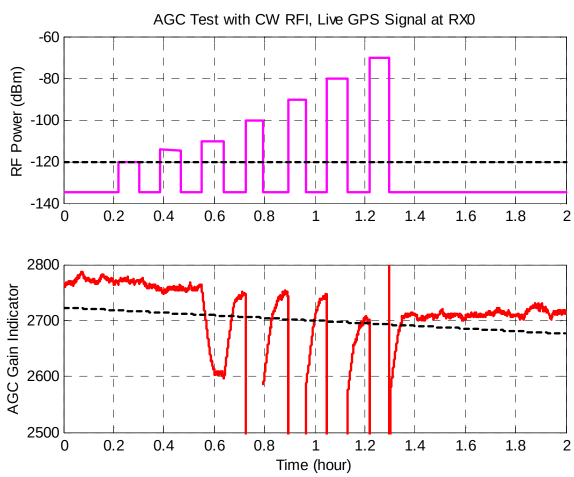

Figure 16: IMT AGC Results with CW RFI

The AGC test results are shown in Figure 16. The plot is zoomed such that the detection points can be clearly seen. In this case, the AGC test statistics triggers the flag when the RFI power is at –110 dBm. This is fairly consistent with the simulator test described in Section 3. Although AGC demonstrates again that it is a sensitive RFI detector, note also the drift of AGC regardless of the presence of RFI. This could be caused by the temperature dependence of RF components, or the stability of other devices in the path. In a LAAS application, this draft has to be calibrated out or otherwise accommodated in order to take full advantage of the AGC observability.

5.0 CONCLUSIONS AND FUTURE WORK

In this paper, the performance of a test receiver has been evaluated relative to the RTCA MOPS RFI mask. A number of different RFI detectors have been tested. It was found that receiver common observables (C/N_0, cycle slip, loss-of-lock) performed as expected. The IMT SNR monitor can detect RFI in a similar fashion to C/N_0. In these tests, the IMT MQM and Innovation monitors responded to RFI only as a second-order effect – the variance of the test statistics increase with the presence of RFI. In most cases, they are not better RFI detectors than receiver's loss-of-lock indicator. However, it is not clear that the scenarios tested actually led to anything approaching hazardous errors (or even significant increases in noise) in code or carrier-phase ranging measurements. AGC outputs were, in general, the most sensitive detectors of both WB and CW RFI. They can be also used as an RFI estimator to help the IMT separate RFI from other failure modes.

Future work will include completing the additional test cases listed in Table 1, including narrow band RFI and pulsed RFI. In addition, more realistic RFI scenarios (e.g., CW interference sweeps across C/A code spectral lines) will be generated to test the IMT with more severe RFI impacts on multiple receivers and verify that EXM is able to distinguish RFI from other types of failures. A longer-term goal is to utilize the receiver AGC outputs to develop an accurate RFI "state estimator" that would allow EXM to better discriminate RFI events that can be tolerated from those that must be alerted.

ACKNOWLEDGMENTS

The authors would like to thank the FAA LAAS Program Office (AND-710) for its support of this research. The opinions expressed here are those of the authors and do not necessarily represent those of the FAA or other affiliated agencies.

REFERENCES

[1] *Global Positioning System - Standard Position System Signal Specification*; 2nd Edition; June 2, 1995.

[2] E. Kaplan, *Understanding GPS: Principles and Applications*. Norwood, MA: Artech House, Inc., 1996.

[3] *Minimum Operational Performance Standards for GPS/Local Area Augmentation System Airborne Equipment*. Washington, D.C., RTCA SC-159, WG-4A, DO-253A, Nov. 28, 2001.

[4] *Minimum Operational Performance Standards for GPS/Wide Area Augmentation System Airborne Equipment.* Washington, D.C., RTCA SC-159, WG-2, DO-229C, Nov. 28, 2001.

[5] *Minimum Aviation System Performance Standards for Local Area Augmentation System (LAAS).* Washington, D.C., RTCA SC-159, WG-4A, DO-245, Sept. 28, 1998.

[6] G. Xie, *et.al*., "Integrity Design and Updated Test Results for the Stanford LAAS Integrity Monitor Testbed(IMT)," *Proceedings of ION 2001 Annual Meeting*. Albuquerque, NM, June 11-13, 2001, pp. 681-693.

[7] P. Enge and A. Ndili, "Interference Mitigation by Stand-Alone and Intrack APLS", Presented to the LAAS Architecture Review Committee, Stanford, OCT. 3-4, 1996.